Supporting Information

Giant metalloorganic M_2L_3 helicate based on phthalocyanines as a host for electroactive molecules

Ettore Fazio,[a] Cally J. E. Haynes,[b] Gema de la Torre,*[a,d] Jonathan R. Nitschke *[b] and Tomás Torres[a,c,d*]

[a] *Departamento de Química Orgánica, Universidad Autónoma de Madrid, 28049 Madrid, Spain.*
E-mail: tomas.torres@uam.es*; Fax:+34 9 1497 3966; Tel: +34 9 1497 4151*
[b] *Department of Chemistry, University of Cambridge, Lensfield Road, Cambridge, CB2 1EW (UK).*
E-mail: jrn34@cam.ac.uk
[c] *IMDEA Nanociencia, c/Faraday, 9, Cantoblanco, 28049 Madrid, Spain.*
[d] *Institute for Advanced Research in Chemical Sciences (IAdChem), Universidad Autónoma de Madrid, 28049 Madrid, Spain*

1. Synthesis and characterization

Chemicals were purchased from commercial suppliers and used without further purification. Column chromatography was carried out on silica gel (Merck, Kieselgel 60, 230–400 mesh, 60 Ä) and TLC was carried out on aluminium sheets pre-coated with silica gel 60 F254 (Merck). Low-resolution electrospray ionization mass spectra (ESI-MS) were obtained on a Micromass Quattro LC. MS (MALDI-TOF) spectra were performed on a BRUKER REFLEX III instrument that was equipped with a nitrogen laser operating at 337 nm and recorded in the positive-polarity mode. High resolution spectra were acquired using a 9.4 T IonSpec QFT-MS FT-ICR mass spectrometer or a Thermofisher LTQ Orbitrap XL hybrid ion trap mass spectrometer. NMR spectra were recorded on a Bruker AC-300 or a Bruker AC-500 or a Bruker Avance DPX 400 MHz, 500 MHz TCI cryoprobe instrument (^{19}F-NMR spectra were acquired with an internal reference). Steady-state absorption spectra were recorded with a Perkin-Elmer Lambda 35. Molecular Modeling

1.1 Synthetic methods

Pc **1**[1] and bis(imidazole)naphthalenediimide derivative **6**[2] were prepared according to literature procedures.

1,4,15,18-Tetrakis(3,5-bis(trifluoromethyl)phenyl)-9,23[24]-bis(3'-hydroxypropyn-1-yl)- zinc (II) phthalocyanine (2a and 2s)

To a solution of **1** (0.119 mmol, 200 mg) in freshly distilled THF (6 mL), Et_3N (2 mL), $Pd(PPh_3)_4$ (10% mol, 14 mg) and CuI (10% mol, 2 mg) were added. The mixture was deoxygenated by bubbling argon through it for 20 min. Propargylic alcohol (0.357 mmol, 20.6 µL) was subsequently added and the mixture was stirred overnight at 50ºC. After evaporation of the solvents, the crude mixture was dissolved in $CHCl_3$ and washed with water. The combined organic layers were dried over $MgSO_4$ and concentrated in vacuum. Purification by column chromatography on silica gel (heptane/THF 5:1) afforded the desired products as blue solids in a 1:1 ratio.

2a: 70 mg, 38% yield
^{1}H-NMR (500 MHz, THF-d_8), δ (ppm): 8.85 (s, 4H), 8.76 (s, 4H), 8.64 (s, 2H), 8.58 (s, 2H), 8.28 (s, 4H), 8.26 (s, 2H), 8.24 (d, J = 5 Hz, 2H), 7.96 (dd, J_1 = 5 Hz, J_2 = 1 Hz, 2H), 4.62 (d, J = 10 Hz, 4H), 4.51 (t, J = 5 Hz, 2H). MS (MALDI) [M+] m/z: 1532.1. UV-Vis (THF) λmax (log ε): 698 (5.05), 678 (5.06), 643 (4.40), 617 (4.40), 360 (4.71), 251 (4.70) nm.

2s:70 mg, 38% yield
^{1}H-NMR (500 MHz, THF-d_8), δ (ppm): 8.83 (s, 4H), 8.79 (s, 4H), 8.64 (s, 2H), 8.58 (s, 2H), 8.29 (s, 2H), 8.28 (s, 2H), 8.27 (s, 2H), 8.21 (d, J = 5 Hz, 2H), 7.96 (dd, J_1 = 5 Hz, J_2 = 1.5 Hz, 2H), 4.62 (d, J = 5 Hz, 4H), 4.51 (t, J = 5, 2H). HR-MS (MALDI) [M+] m/z calculated: 1532.1238, found: 1532.1279. UV-Vis (THF) λmax (log ε): 696 (5.06), 680 (5.08), 641 (4.38), 615 (4.38), 361 (4.70), 253 (4.66) nm.

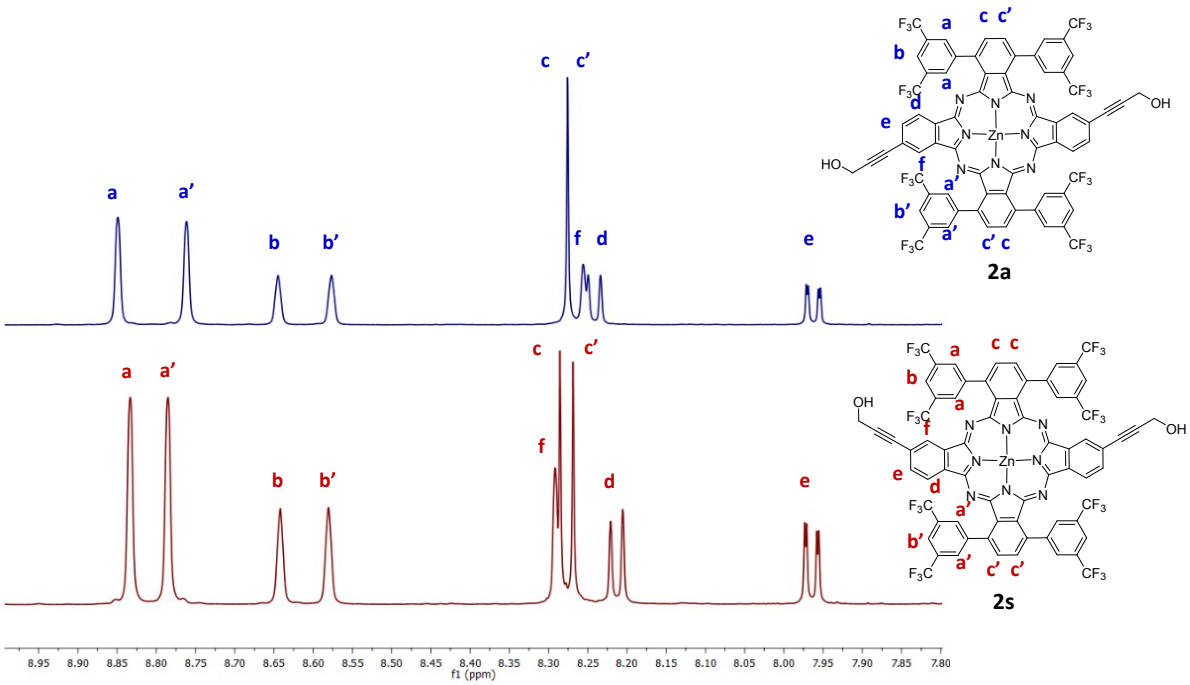

Figure S1. Magnification of the aromatic region of the ^{1}H-NMR spectra in THF-d_8 of **2a** (top) and **2s** (bottom).

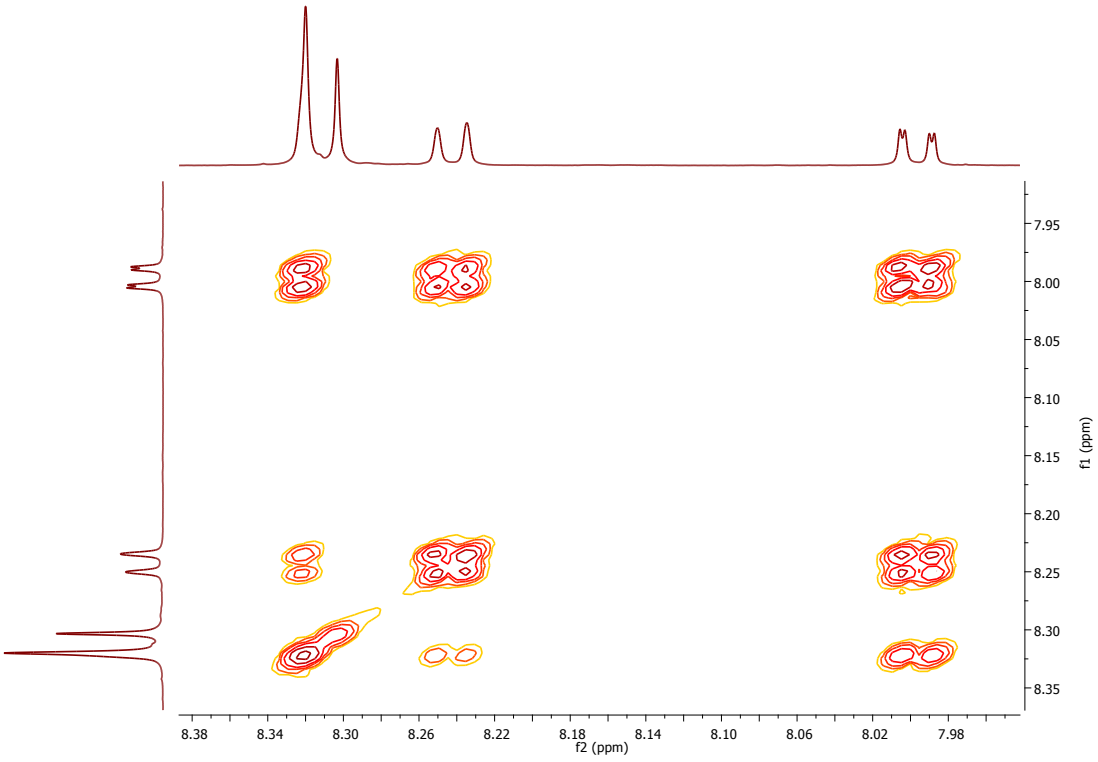

Figure S2. Aromatic region magnification of ^{1}H COSY NMR of **2s** in THF-d_8.

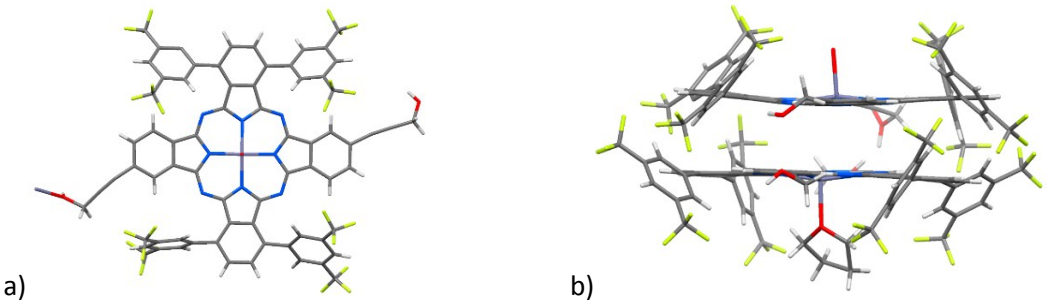

Figure S3. X-ray structure of **2a**. a) Frontal view of the C_{2h} isomer **2a**, in which solvent molecules were omitted for clarity; b) Side view of a stacked dimer of **2a** with a THF molecule.

General procedure for the synthesis of phthalocyanines 3a and 3s

To a solution of phthalocyanine **2a** or **2s** (0.0072 mmol, 11 mg) in Et_2O (2 ml), MnO_2 (0.69 mmol, 60 mg) and recently powdered KOH (0.53 mmol, 30 mg) were added. The mixture was stirred at reflux overnight (the reaction can be easily monitored by TLC with heptane/THF 3:1). Then, the solid was filtered off and washed with Et_2O. The filtrate was concentrated to dryness. Then the crude mixture was dissolved in CH_2Cl_2 and washed with water. Purification by column chromatography on silica gel (heptane/THF 3:1) afforded the desired products.

1,4,15,18-Tetrakis(3,5-bis(trifluoromethyl)phenyl)-9,24-diethynyl zinc(II) phthalocyanine (3s)

Blue solid (9 mg, 86% yield).

^{1}H-NMR (300 MHz, THF-d_8), δ (ppm): 8.88 (s, 4H), 8.85 (s, 4H), 8.63 (s, 2H), 8.59 (s, 2H), 8.39 (s, 2H), 8.34 (s, 2H), 8.32 (s, 2H), 8.28 (d, J = 9 Hz, 2H), 8.08 (dd, J_1 = 9 Hz, J_2 = 1.2 Hz, 2H), 4.0 (s, 2H). HR-MS (MALDI) [M+] m/z calculated: 1472.1027, found: 1472.1058. UV-Vis (THF) λmax (log ε): 693 (5.06), 679 (5.06), 640 (4.37), 614 (4.40), 356 (4.71), 243 (4.80), 215 (4.87) nm.

1,4,15,18-Tetrakis(3,5-bis(trifluoromethyl)phenyl)-9,23-diethynyl zinc(II) phthalocyanine (3a)

Blue solid (9 mg, 86% yield).

^{1}H-NMR (300 MHz, THF-d_8), δ (ppm): 8.85 (s, 4H), 8.80 (s, 4H), 8.59 (s, 2H), 8.55 (s, 2H), 8.33 (s, 2H), 8.29 (s, 4H), 8.25 (d, J = 9 Hz, 2H), 8.04 (dd, J_1 = 9 Hz, J_2 = 0.9 Hz, 2H), 3.97 (s, 2H). MS (MALDI) [M+] m/z: 1472.1. UV-Vis (THF) λmax (log ε): 694 (5.07), 678 (5.06), 642 (4.37), 615 (4.39), 354 (4.69), 245 (4.77), 214 (4.89) nm.

General procedure for the synthesis of phthalocyanines 4a and 4s

Phthalocyanine **3s** or **3a** (0.03 mmol, 40 mg), 4-Iodoaniline (0.09 mmol, 20 mg), $Pd(PPh_3)_4$ (5% mol, 2 mg) and CuI (5% mol, 0.3 mg) were dissolved in freshly distilled THF (3 mL) and Et_3N (1 mL). The mixture was stirred 3 hours at 60ºC. After evaporation of the solvents, the crude mixture was dissolved in $CHCl_3$ and washed with water. The combined organic layers were dried over $MgSO_4$ and concentrated in vacuum. Purification by column chromatography on silica gel (heptane/AcOEt 1:1) and precipitation with heptane afforded the desired product.

1,4,15,18-Tetrakis(3,5-bis(trifluoromethyl)phenyl)-9,24-bis(4,4'-dianilinethynyl) zinc(II) phthalocyanine (4s)

Green solid (41 mg, 83% yield).

^{1}H-NMR (300 MHz, THF-d_8), δ (ppm): 8.83 (s, 8H), 8.59 (s, 4H), 8.30 (s, 2H), 8.28 (s, 2H), 8.26 (s, 2H), 8.20 (d, J = 9 Hz, 2H), 7.99 (dd, J = 9 Hz, 2H), 7.48 (d, J = 9 Hz, 4H), 6.71 (d, J = 9, 4H). HR-MS (MALDI) [M+] m/z calculated: 1654.1871, found: 1654.1900. UV-Vis (THF) λmax (log ε): 696 (5.25), 628 (4.58), 358 (4.87), 253 (4.78), 215 (4.92) nm.

1,4,15,18-Tetrakis(3,5-bis(trifluoromethyl)phenyl)-9,23-bis(4,4'-dianilinethynyl) zinc(II) phthalocyanine (4a)

Green solid (40 mg, 83% yield).

^{1}H-NMR (300 MHz, THF-d_8), δ (ppm): 8.85 (s, 4H), 8.81 (s, 4H), 8.58 (s, 4H), 8.26 (s, 6H), 8.20 (d, J = 9 Hz, 2H), 7.98 (dd, J = 9 Hz, 2H), 7.49 (d, J = 9 Hz, 4H), 6.72 (d, J = 9, 4H). MS (MALDI) [M+]

m/z: 1654.2. UV-Vis (THF) λmax (log ε): 696 (5.25), 626 (4.58), 359 (4.88), 253 (4.78), 213 (4.95) nm.

Assembly of Fe_2L_3 helicate 5

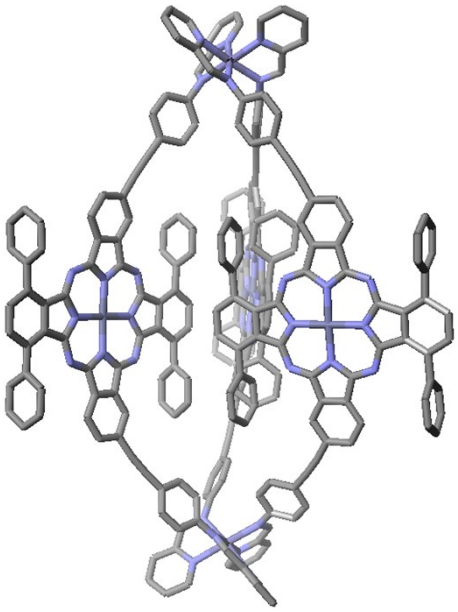

4s (2.0 mg, 1.21 µmol), $Fe(OTf)_2$ (0.3 mg, 0.81 µmol) and 2-formylpyridine (24 µL of a stock solution 0.1 M in CD_3CN, 2.42 µmol) were dissolved in deuterd MeCN (0.6 mL) in a J-Young nmr tube. The solution was degassed by three evacuation/nitrogen fill cycles and, then, sonicated for 30 minutes. The resultant dark green solution was left at room teperature for 24 h. Then, the dropwise addition of Et_2O precipitates the desired product, which was collected by filtration and washed with additional Et_2O, then redissolved in MeCN (1 mL). The solution was reduced to dryness to give a green powder (2 mg, 0.32 µmol, 80 %).

^{1}H-NMR (400 MHz, CD_3CN), δ (ppm): 9.2 (s, 2H), 8.8 (s, 4H), 8.7 (d, J = 7.2 Hz, 2H), 8.55 – 8.51 (,m 8H), 8.2 (s, 2H), 8.08 – 8.03 (m, 4H), 8.0 (s, 2H), 7.93 – 7.89 (m, 6H), 7.7 (d, J = 8.4 Hz, 4H), 7.6 (d, J = 5.6 Hz, 2H), 5.7 (d, J = 7.6 Hz, 4H).

LR-ESI-MS [charge calculated for $C_{276}H_{120}F_{72}Fe_2N_{36}Zn_3(OTf)_4$] *m/z* : 1919.4 [**5**$(OTf)^{3+}$, 1919.2], 1402.4 [**5**$^{4+}$, 1402.1]. HR-MS (ESI-TOF) *m/z* calculated for [**5**]$^{4+}$: 1402.1486, found: 1402.0856.

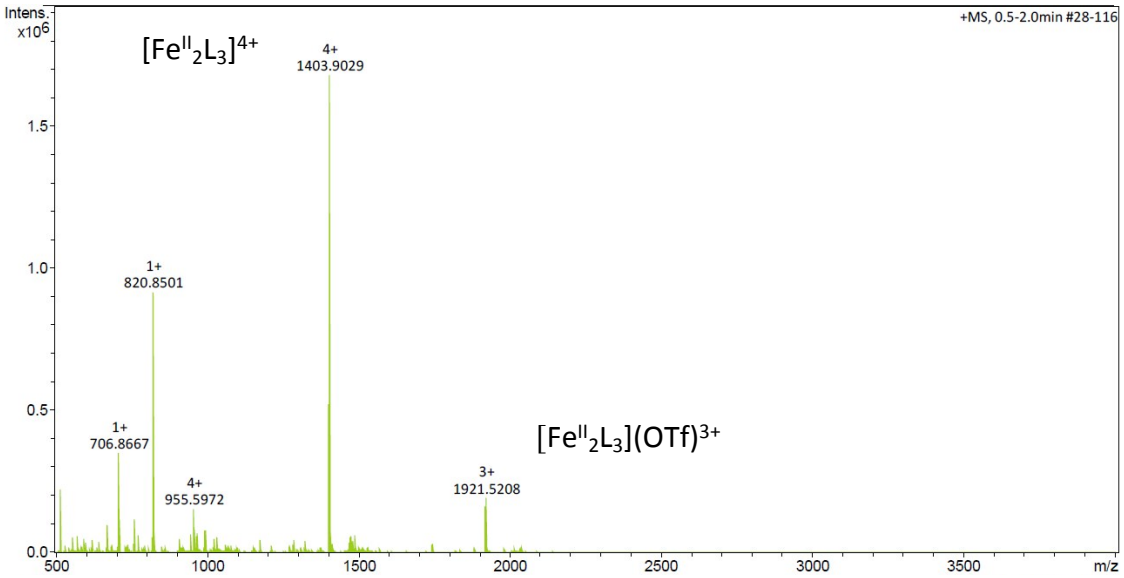

Figure S4: High resolution ESI mass spectrum of **5**, showing two of the three possible peaks at *m/z* = 1403.9029 for $[Fe^{II}_2L_3]^{4+}$ and *m/z* = 1921.5208 for the helicate-counterion complexes $[Fe^{II}_2L_3](OTf)^{3+}$.

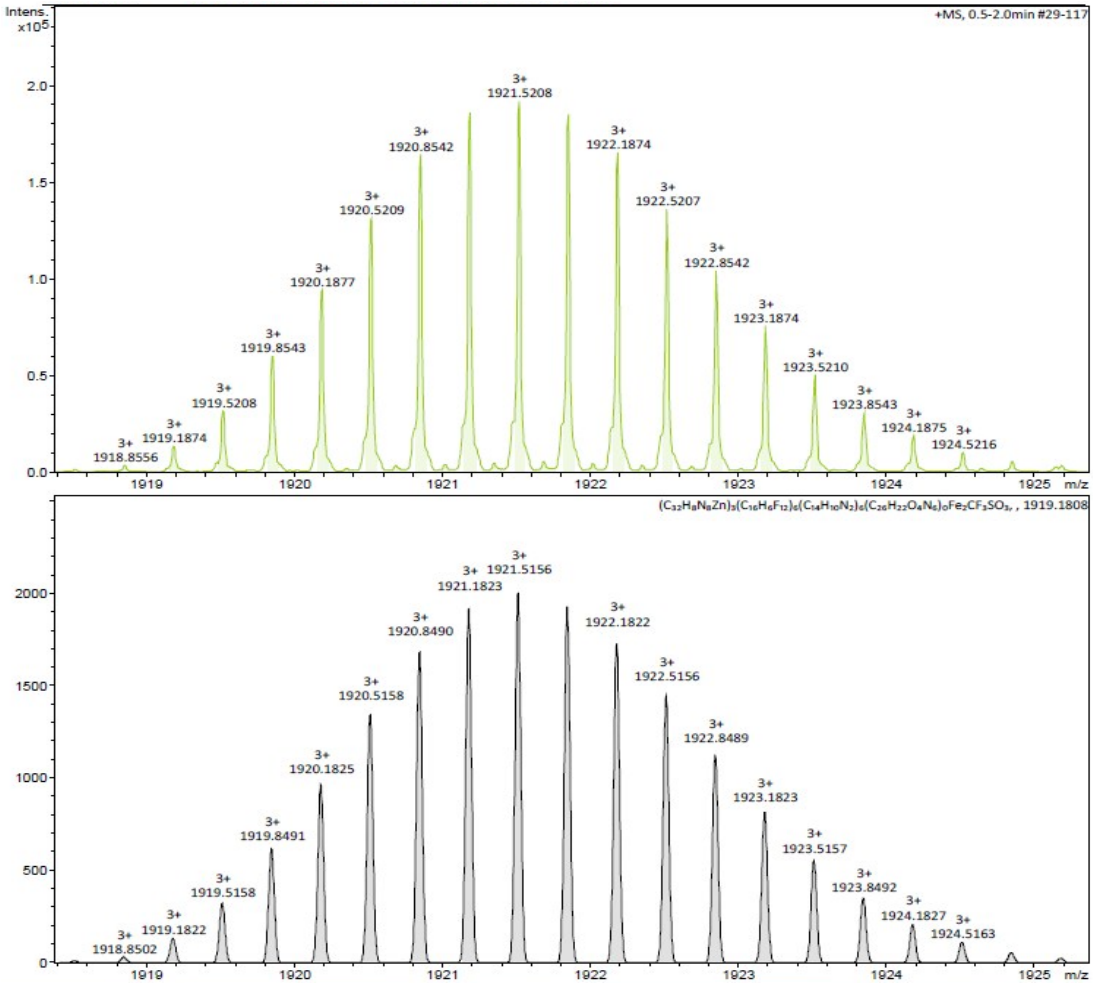

Figure S5: High resolution ESI mass spectrum of **5**, showing the observed *z* = +3 charge for the peak at *m/z* = 1921.5208 (bottom) compared to the theoretical isotopic pattern (top).

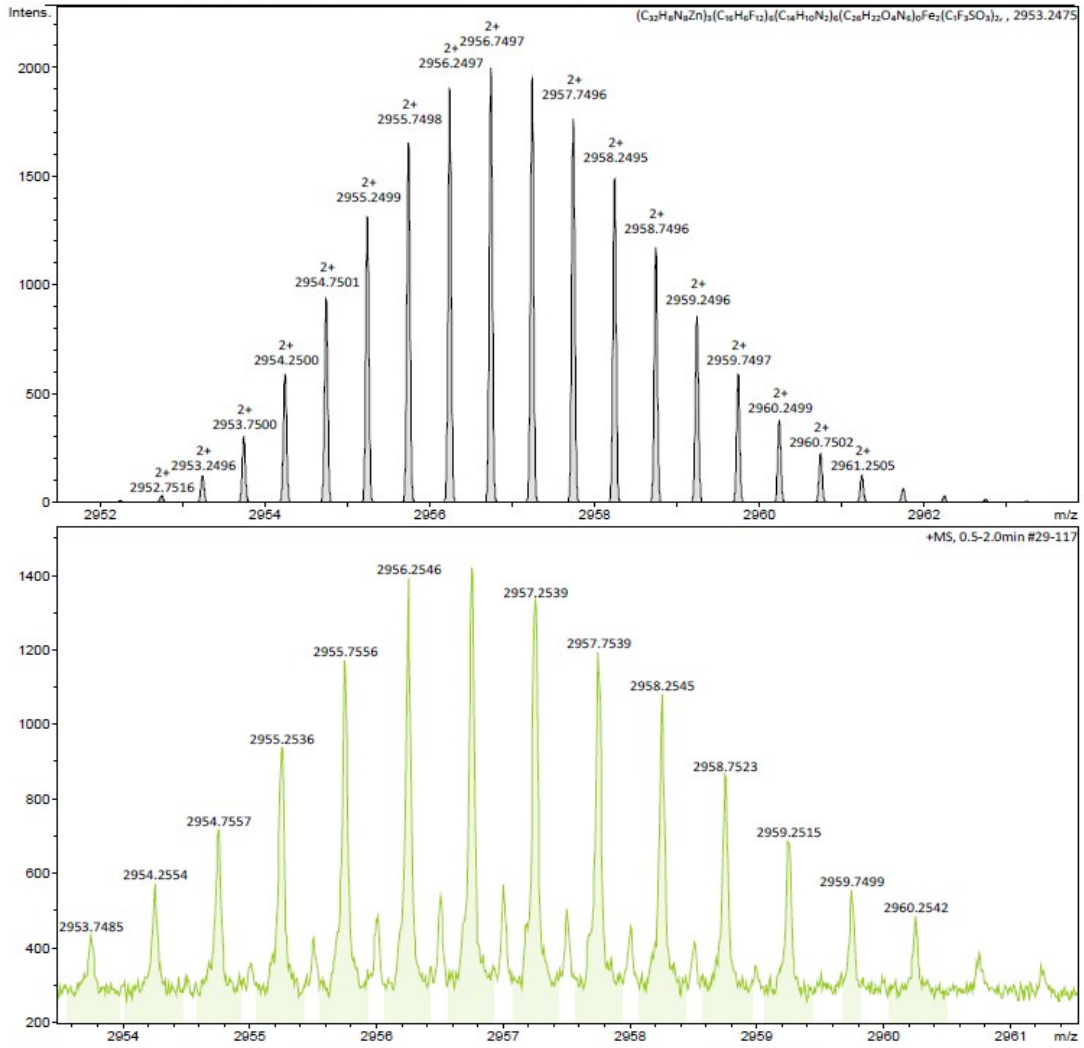

Figure S6: High resolution ESI mass spectrum of **5**, showing the observed *z* = +2 charge for the peak at *m/z* =2956.2546 (bottom) compared to the theoretical isotope pattern (top).

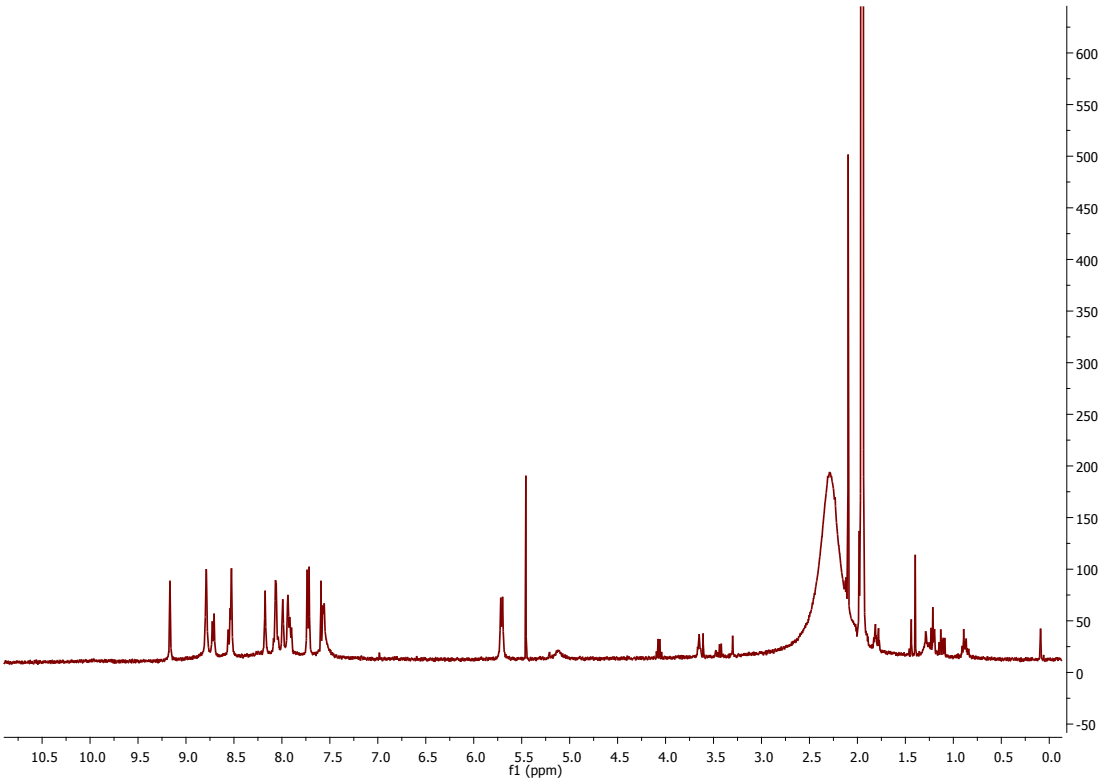

Figure S7: ^{1}H-NMR (400 MHz, CD_3CN) spectrum of **5**.

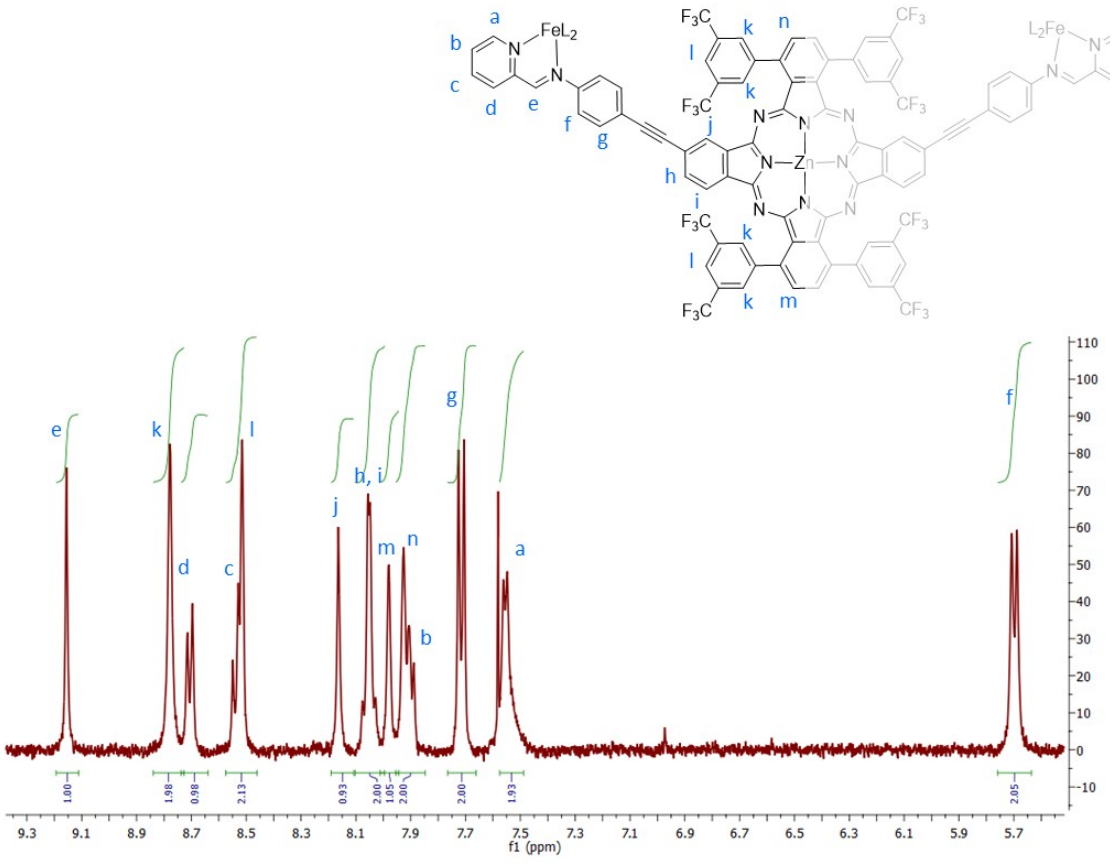

Figure S8: Aromatic region magnification of ^{1}H-NMR (CD_3CN) spectrum of **5**.

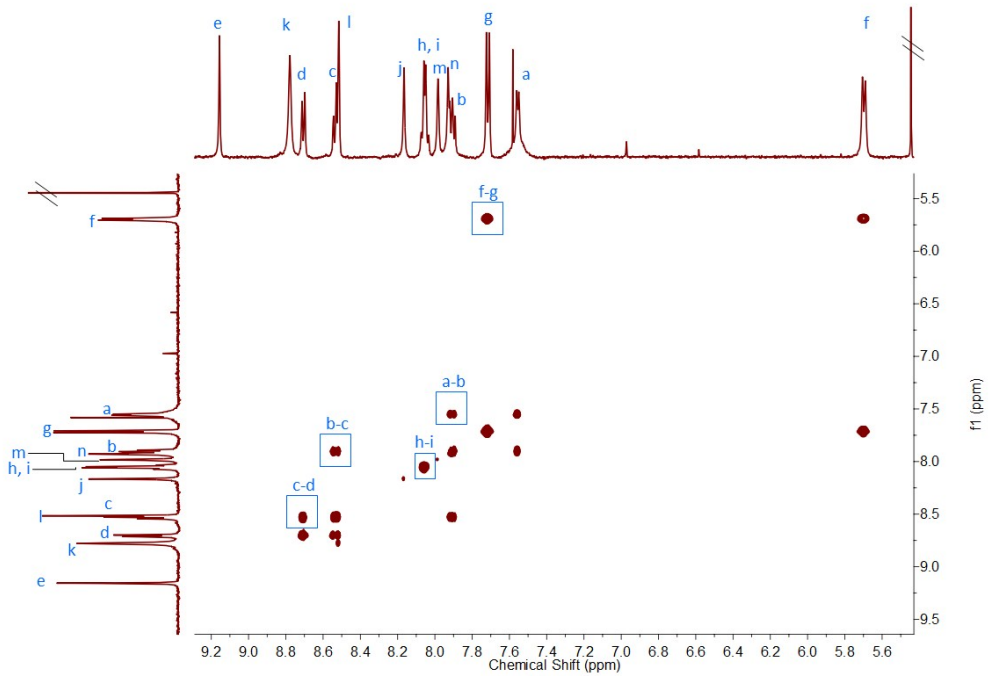

Figure S9: Aromatic region of the COSY (CD_3CN) spectrum of **5**.

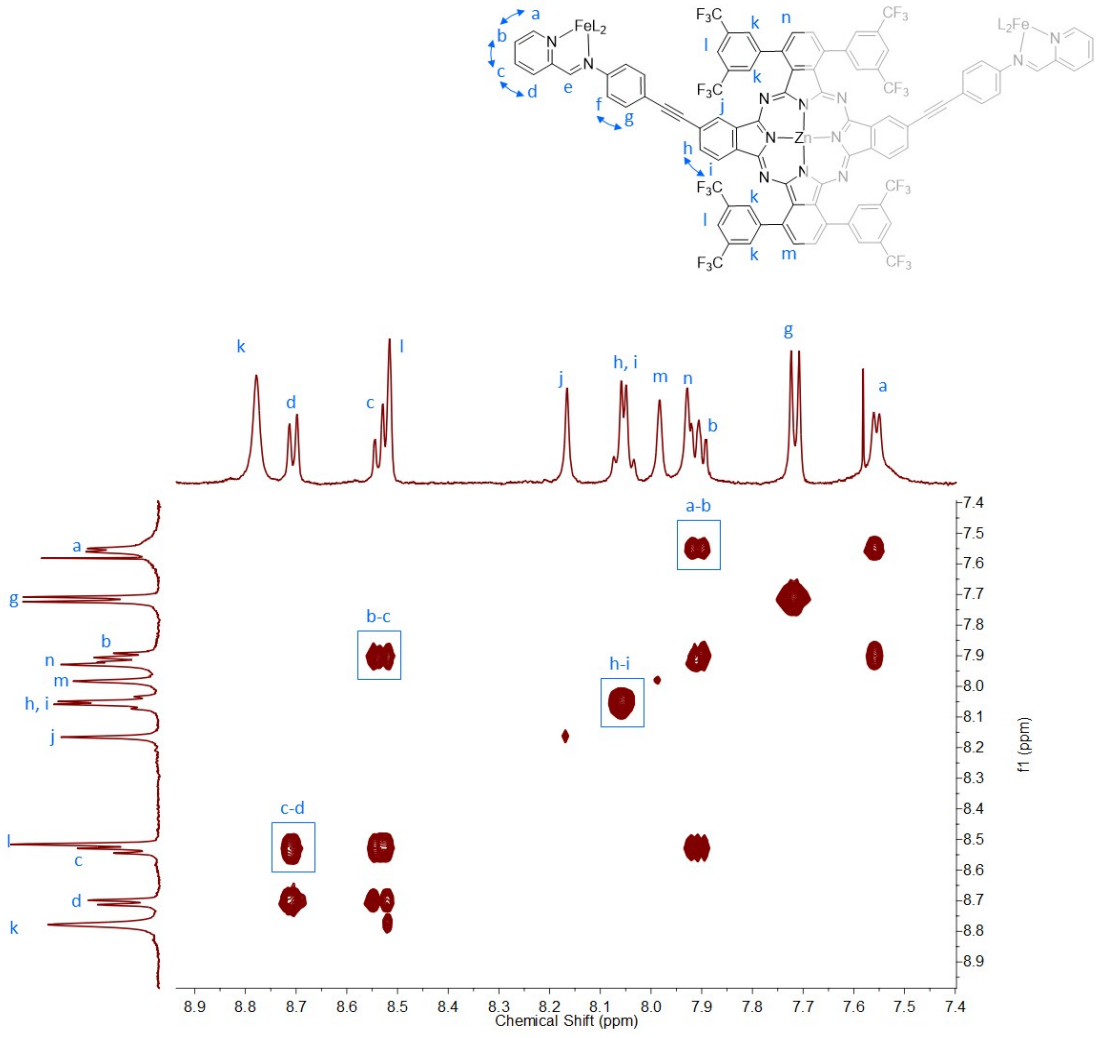

Figure S10: Aromatic region magnification of the COSY (CD_3CN) spectrum of **5**.

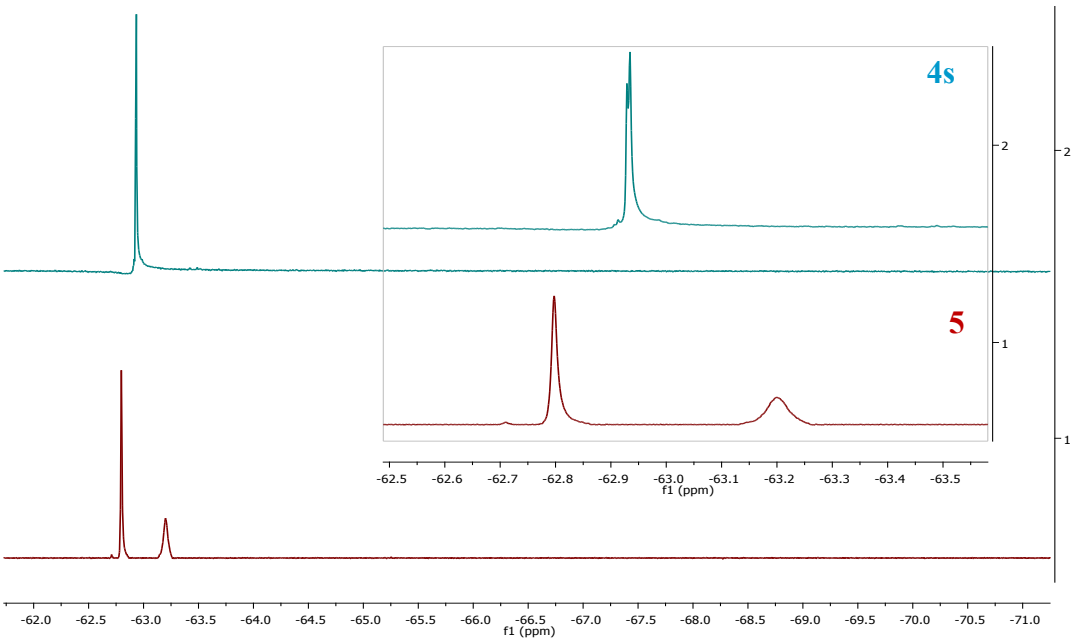

Figure S11: Comparison of ^{19}F-NMR (400 MHz) spectra of **4s** (THF – blue line) and **5** (CD_3CN – red line).

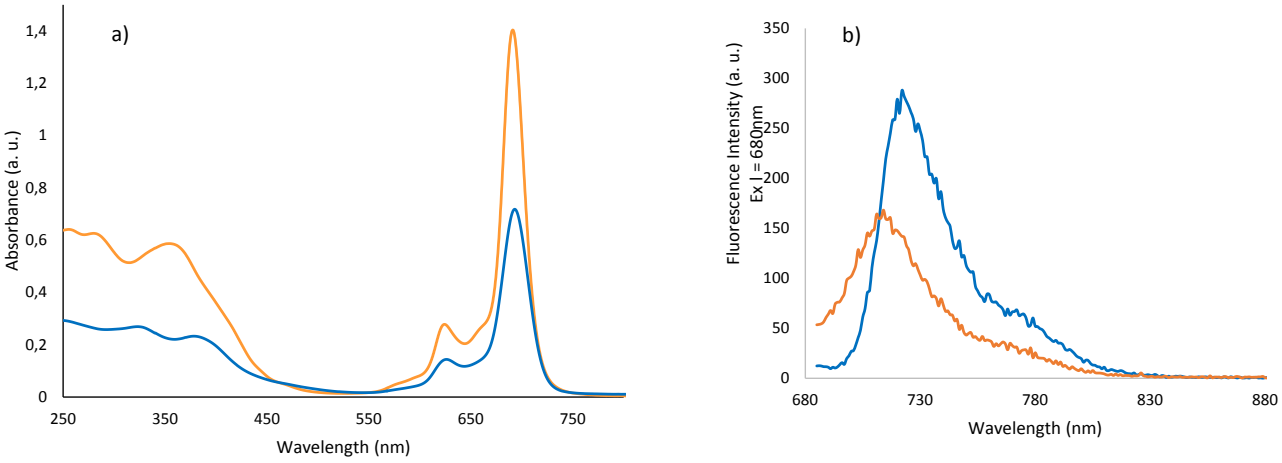

Figure S12. a) UV-vis spectra of Pc **4s** (blue line, 5 µm) in THF and **5** (orange line, 10 µm) in CH_3CN. b) Fluorescence spectra of Pc **4s** (blue line, 30µM) in $CHCl_3/CH_3CN$ (1:20) and **5** (orange line, 10µM) in CH_3CN.

1.2 Estimation of the helicate size

Diffusion ordered spectroscopy (DOSY) was carried out in the presence of mesitylene as reference compound (**R**) to calculate the hydrodynamic radius (R_h) of **5** in solution.
Diffusion coefficients (*D*) are related to the effective radius of the molecular species through the Stokes– Einstein equation (Eq. S1): [3,4]

$$D = \frac{k_B T}{6\pi\eta R_h} \qquad \text{Eq.S1}$$

where k_B is the Boltzmann's constant, *T* the temperature and η is the viscosity of the solvent. The Stokes–Einstein equation is a reasonable approximation to measure the radius of many cages and organometallic capsules that are relatively large (compared to the solvent molecules), and that possess various similar axes.[5,6] It is important to note that R_h represents the hydrodynamic size, and such is a measure related to the nature of the solvent in which the diffusion occurs. In fact, it represents the radius of a hypothetical hard sphere that diffuses with the same speed as the examined particle, and therefore possess some redundancy.
That said, it should be noted that the Eq. S1 is valid only for hard spheres, and for this reason a modified Stokes–Einstein equation (Eq. S2) should be used for molecular and supramolecular architectures with non-spherical structure. This equation takes into account the deviations from the hard sphere approximation and the deviation from the continuum fluid approximation of the starting Eq. S1:

$$D = \frac{k_B T}{c\pi\eta R_h f_h} \qquad \text{Eq.S2}$$

where f_h is the shape factor and is always greater than unity, while *c* is the size factor and relates to the ratio of the size of the diffusing entity to the solvent in which diffusion occurs. The shape factor f_h was computed for prolate and oblate ellipsoids,[7] for ellipsoids having three different axes[8]. Nevertheless, different works in literature show that, despite the fact that many of the helicates are clearly not spherical, the differences between data calculated using the Stokes–Einstein equation (Eq. S1) and obtained by X-ray structures of the complexes are in the order of 10–15%,[9,10] therefore negligible.
For these reasons, we assume that, also in our case, diffusion coefficients can be used to determine the size of our supramolecular structure, according to the previously reported methodologies in literature.[11-13] The use of mesitylene as internal reference, with a well-established hydrodynamic radius (R_{ref} = 3.0 Å), allows for the estimation of the aggregate size by direct D_0 comparison, using equation S3:[12,14]

$$R_0 = \frac{R_{ref} \times D_{ref}}{D_0} \qquad \text{Eq.S3}$$

The calculated diffusion coefficients and the estimated hydrodynamic radii are shown in the following table.

Table S1.

	Peak	**D_0**	**R[a]**	**R[b]**
	ppm	m^2/s	Å	Å
Helicate **5**	9.86	3.306×10^{-12}	17.23	**15.9**
	8.81	3.645×10^{-12}	15.63	
	8.74	3.489×10^{-12}	16.33	
	8.08	3.784×10^{-12}	15.05	
	7.74	3.973×10^{-12}	14.34	
Average *R*			**15.7**	

Mesitylene	6.70	3

[a] Calculated using mesitylene as an internal reference. [b] Calculated from computed models.

An average experimental radius of 15.7 Å was determined for **5**, which is consistent with the value of 15.9 Å derived from the model shown in in Figure S13.

In this model the helical structure of **5** is approximated to a prolate spheroid described by two semi-axes *a* and *b* (Figure S13a). The semi-axis *b* is the distance from center to pole along the symmetry axis and is estimated as the average half-distance between two opposite pyridines among the six iron-coordinating ligands (Figure S13b). On the other hand, the semi-axis *a* is the equatorial radius of the spheroid, and can be estimated as the radius of the circumscribed circle of the triangle obtained combining Pc-centered opposite and extreme hydrogen atoms of the three Pcs forming the helicate (Figure S13c). Using this modelling, values of 14.3 Å and 17.5 Å were calculated for semi-axes *a* and *b* respectively. The average measure of these two values (i.e. 15.9 Å) can be used as approximation of hydrodynamic radius for **5**.

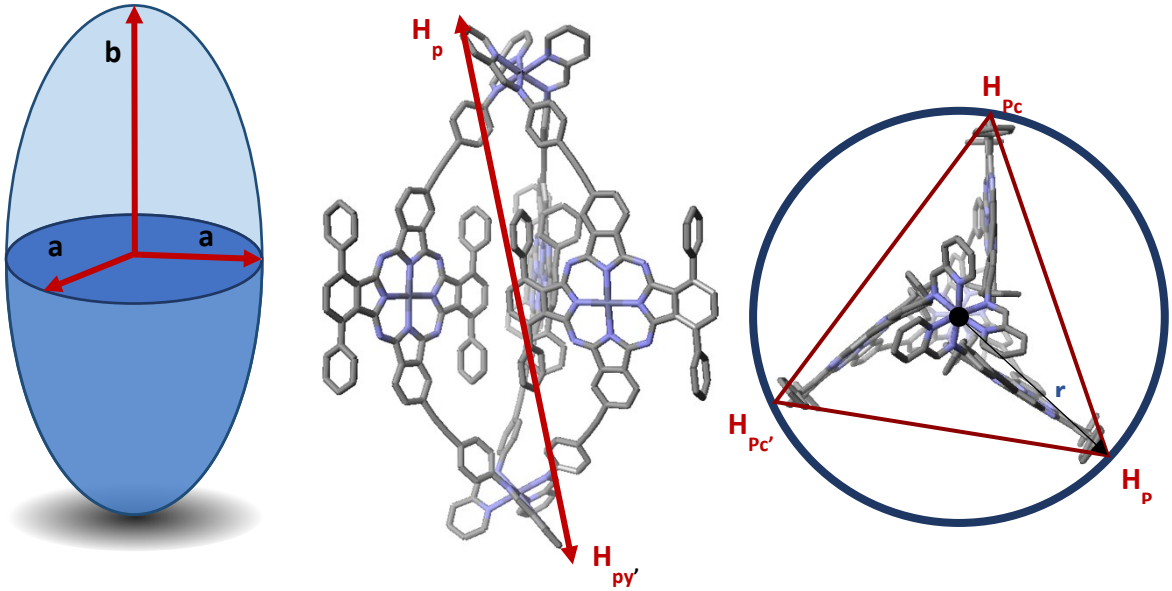

a) b) c)

Figure S13. Schematic representation of a) a prolate spheroid described by the semi-axes *a* and *b*; b) the distance between two opposite pyridines; c) the radius of the circumscribed circle of the triangle obtained combining Pc-centered opposite and extreme hydrogen atoms.

1.3 Void space volume calculation

In order to determine the size of the inner cavity of **5**, VOIDOO [15] calculations based on the optimized structure were performed. A virtual probe with a radius of 3.0 Å was used, and the following parameters were changed from their default settings:

Maximum number of volume-refinement cycles:		30
Maximum number of detection cycles:	30	
Minimum size of secondary grid:		1
Grid for plot files:		0.2
Primary grid spacing:		0.2

The cavity was visualised as a green mesh inside the optimized structure of **5**.

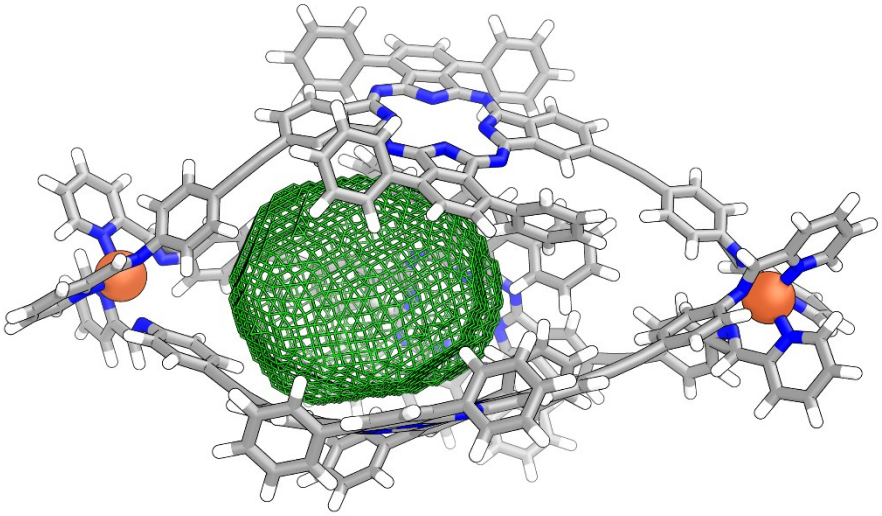

Figure S14. Representation of the internal cavity volume (705,228 $Å^3$ ± 1,182) calculated with VOIDOO

Because of the arching structure of one of the Pc ligands in the model, the Voidoo volume value should be treated cautiously. As shown in Figure S16, the probe simulation did not get into the corners of the structure because of one quite open face of the helicate model, which avoids the use of smaller probes. The cavity size is highly dependent on the orientation and bending of the ligands, and therefore, it could be slightly variable.

2. Host-Guest Chemistry

2.1 Preparation and characterisation of [C_{60} ⊂ **5**]

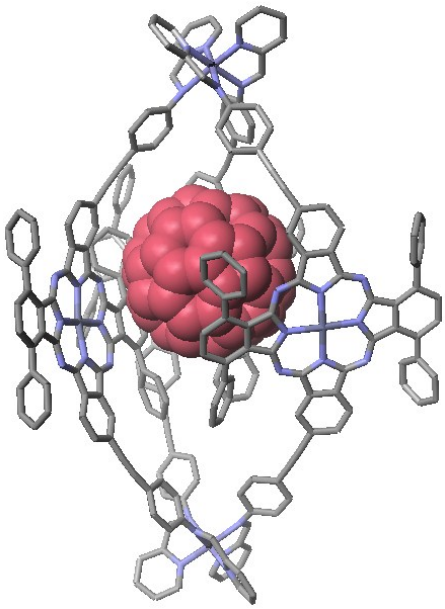

4s (2.0 mg, 1.21 µmol), $Fe(OTf)_2$ (0.3 mg, 0.81 µmol) and 2-formylpyridine (24 µL of a stock solution 0.1 M in CD_3CN, 2.42 µmol) were dissolved in deuterd MeCN (0.6 mL) in a J-Young NMR tube to yield **5** as in the previous conditions. C_{60} (0.6 mg, 0.8 µmol) was added to the solution and the mixture was sonicated, followed by heating at 70˚C for 16 h. Then, the solution was filtred to remove the unreacted C_{60}.

^{1}H-NMR (400 MHz, CD_3CN), δ (ppm): 9.2 (s, 2H), 8.9 (s, 4H), 8.7 (d, J = 8 Hz, 2H), 8.55 – 8.52 (,m 8H), 8.2 (s, 2H), 8.08 – 8.03 (m, 4H), 8.0 (s, 2H), 7.93 – 7.89 (m, 6H), 7.7 (d, J = 8 Hz, 4H), 7.6 (d, J = 4 Hz, 2H), 5.7 (d, J = 8 Hz, 4H). HR-MS (ESI-TOF) *m/z* calculated for [C_{60} ⊂ **5**]$^{4+}$: 1582.3989, found: 1532.3343.

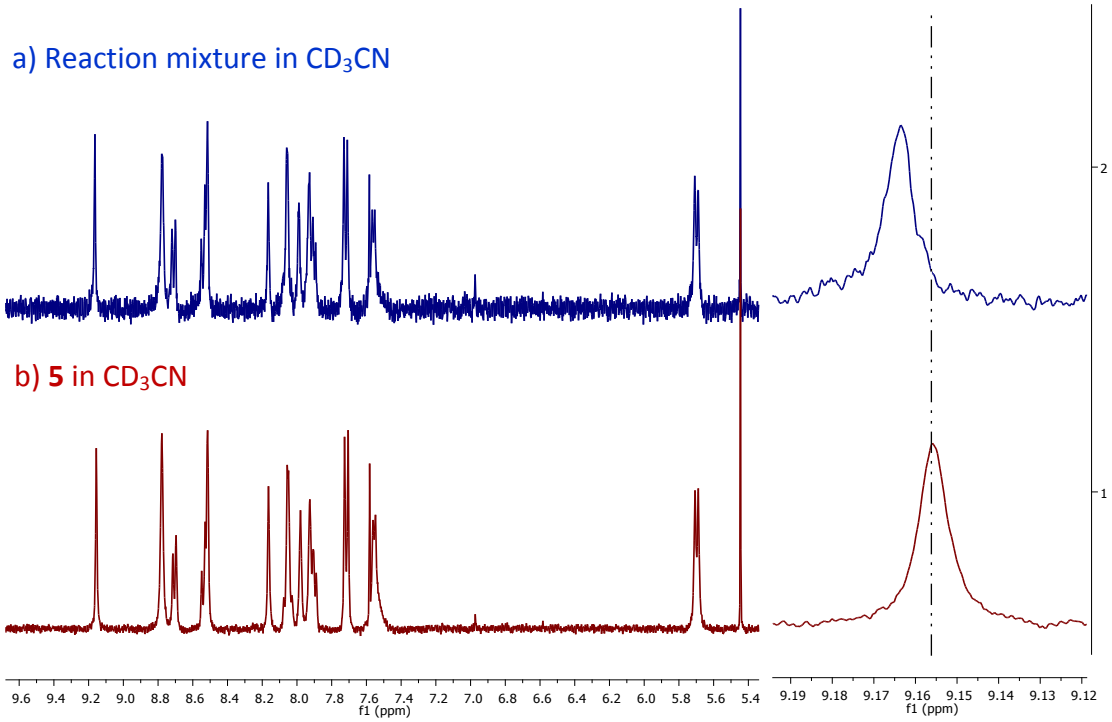

Figure S15: Comparison of the ^{1}H-NMR spectra for the reaction mixture containing [C_{60} ⊂ **5**] (a-top) and empty **5** (b-bottom). **Left:** aromatic region where host peaks are located; **right:** expansion of the imine peak region showing the different chemical shifts for each species.

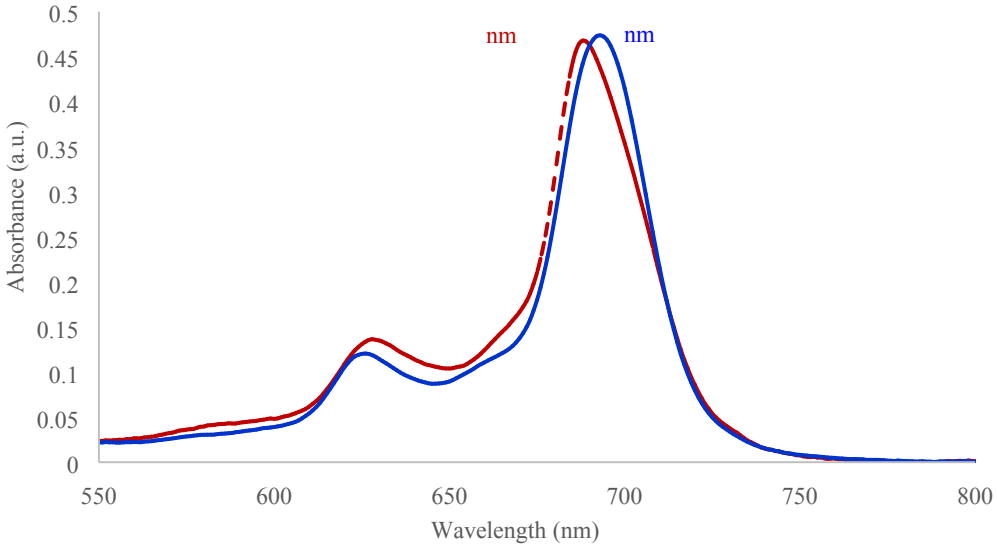

Figure S16: UV-vis spectra in CH_3CN. Comparison of the Q-bands for the reaction mixture containing $[C_{60} \subset \mathbf{5}]^{4+}$ (solid line) and empty **5** (dashed line).

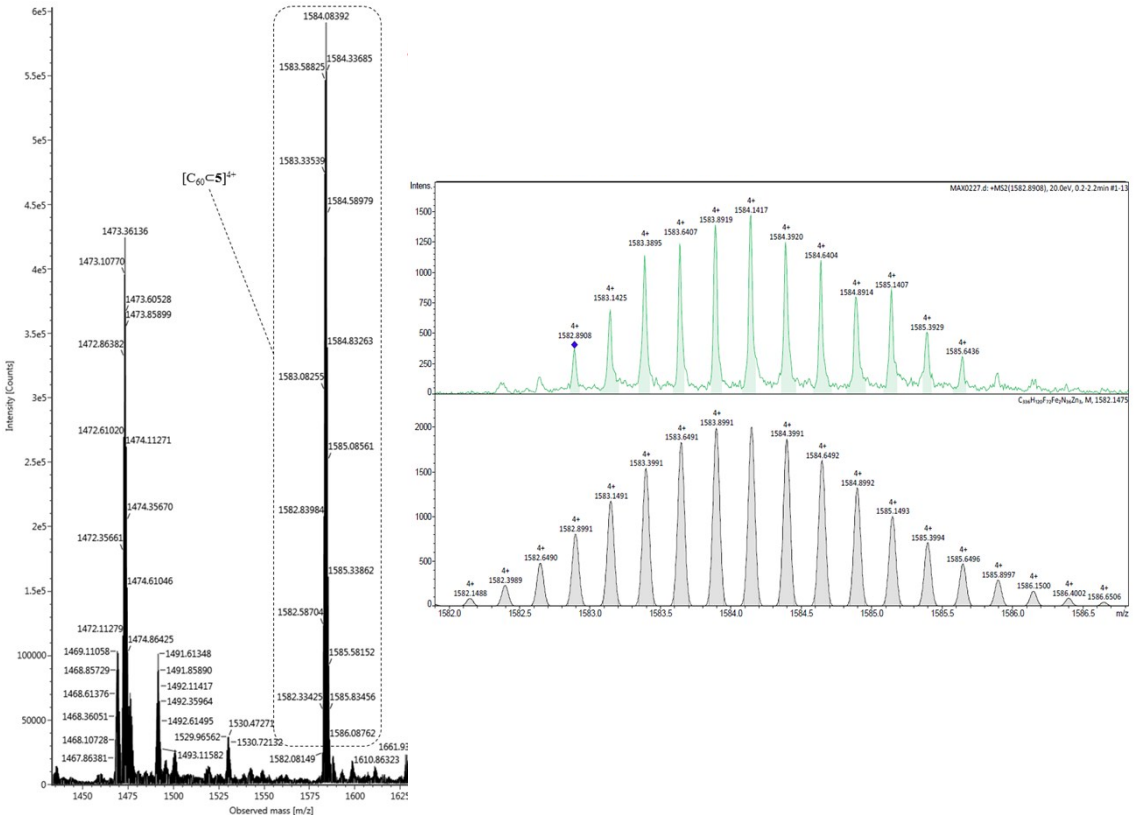

Figure S17: High resolution ESI mass spectrum of $[C_{60} \subset \mathbf{5}]$, showing the observed z = +4 charge for the peak at m/z = 1584.1417 (top) compared to the theoretical isotope pattern (bottom).

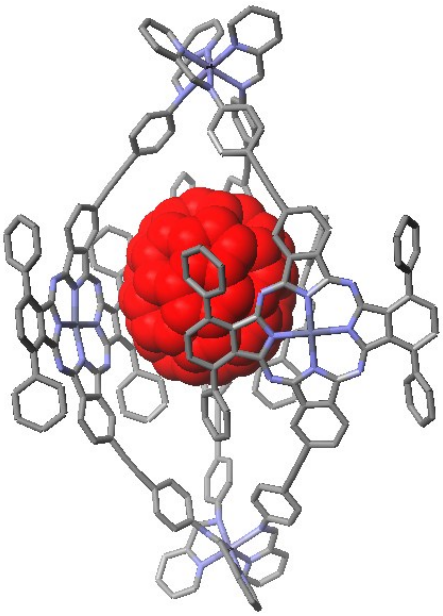

2.2 Preparation and characterization of [C_{70} ⊂ **5**]

4s (2.0 mg, 1.21 µmol), $Fe(OTf)_2$ (0.3 mg, 0.81 µmol) and 2-formylpyridine (24 µL of a stock solution 0.1 M in CD_3CN, 2.42 µmol) were dissolved in deuterd MeCN (0.6 mL) in a J-Young NMR tube to yield **5** as in the previous conditions. C_{70} (0.7 mg, 0.8 µmol) was added to the solution and the mixture was sonicated, followed by heating at 70˚C for 16 h. Then, the solution was filtred to remove the unreacted C_{70}.

^{1}H-NMR (400 MHz, CD_3CN), δ (ppm): 9.2 (s, 2H), 8.8 (s, 4H), 8.7 (d, J = 8 Hz, 2H), 8.55 – 8.52 (,m 8H), 8.2 (s, 2H), 8.08 – 8.03 (m, 4H), 8.0 (s, 2H), 7.93 – 7.89 (m, 6H), 7.7 (d, J = 8 Hz, 4H), 7.6 (d, J = 5 Hz, 2H), 5.7 (d, J = 8 Hz, 4H). HR-MS (ESI-TOF) *m/z* calculated for [C_{70} ⊂ **5**]$^{4+}$: 1612.1489, found: 1612.1438.

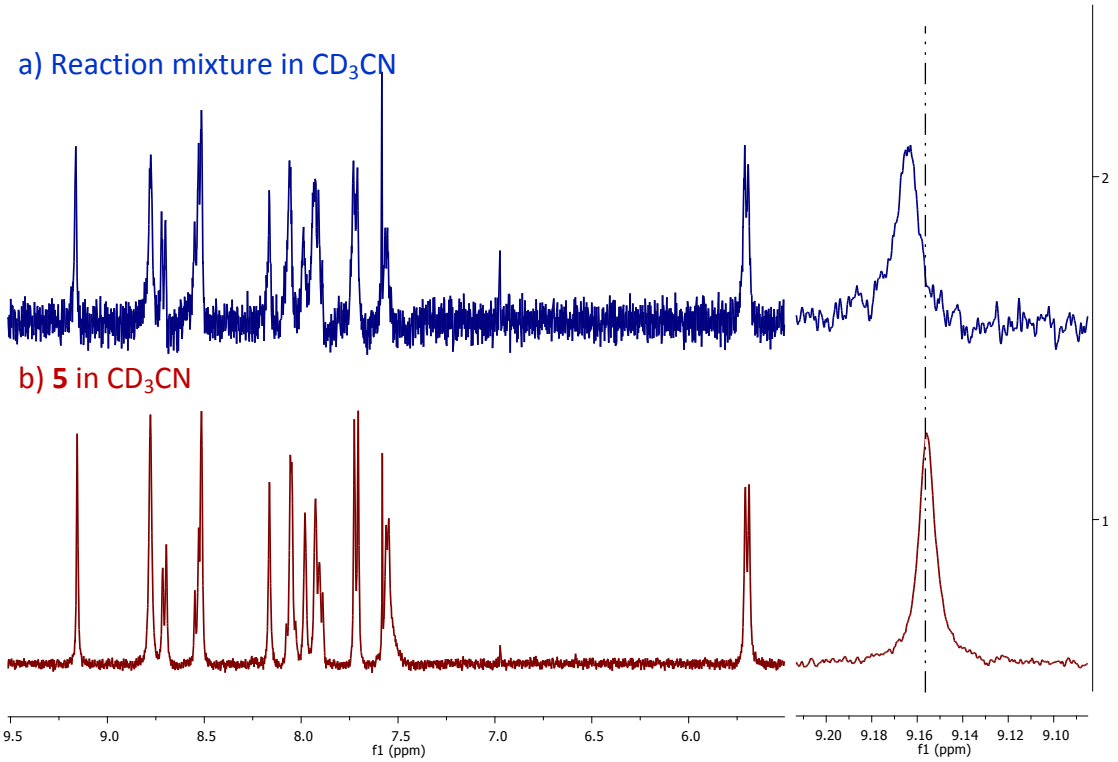

Figure S18: Comparison of the ^{1}H-NMR spectra for the reaction mixture containing [C_{70} ⊂ **5**] (a-top) and empty **5** (b-bottom). **Left:** aromatic region where host peaks are located; **right:** expansion of the imine peak region showing the different chemical shifts for each species.

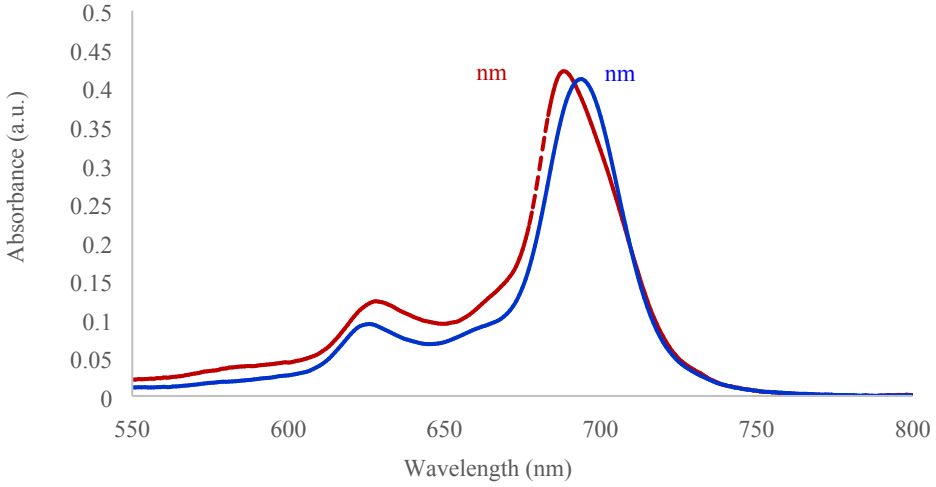

Figure S19: UV-vis spectra in CH_3CN. Comparison of the Q-bands for the reaction mixture containing [C_{70} ⊂ **5**] (solid line) and empty **5** (dashed line).

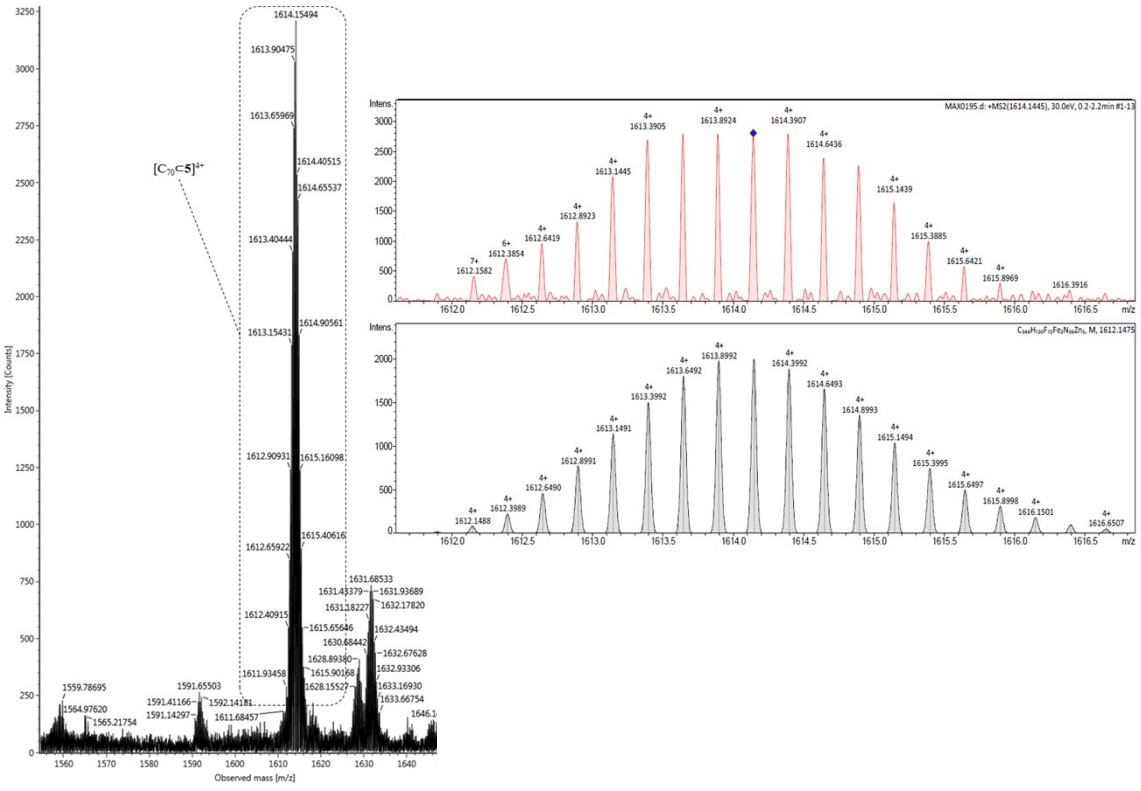

Figure S20: High resolution ESI mass spectrum of [C_{70} ⊂ **5**], showing the observed *z* = +4 charge for the peak at *m/z* = 1613.8924 (top) compared to the theoretical isotope pattern (bottom).

2.3 Preparation and characterization of [6 ⊂ 5]

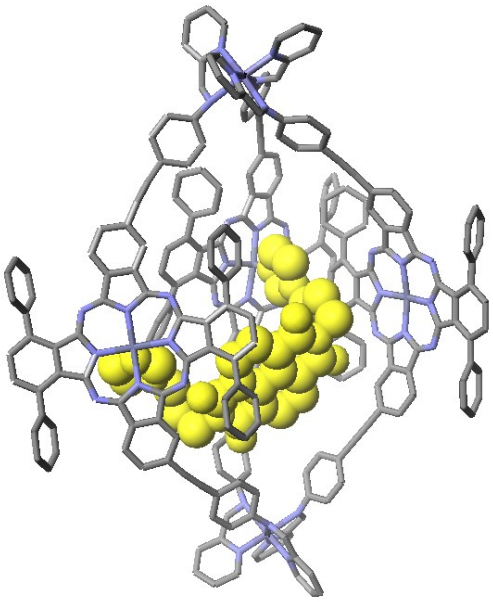

4s (2.0 mg, 1.21 µmol), $Fe(OTf)_2$ (0.3 mg, 0.81 µmol) and 2-formylpyridine (24 µL of a stock solution 0.1 M in CD_3CN, 2.42 µmol) were dissolved in deuterd MeCN (0.6 mL) in a J-Young nmr tube to yield **5** as in the previous conditions. Bis-imidazole NDI derivate **6** (0.32 µmol, 12 µl of a stock solution 26 mM in $CDCl_3$) was added to the solution and the mixture was sonicated. Then, the solution was filtred.

^{1}H-NMR (400 MHz, CD_3CN), δ (ppm): 9.2 (s, 2H), 8.8 (s, 4H), 8.7 (d, J = 8 Hz, 2H), 8.55 – 8.51 (,m 10H), 8.2 (s, 2H), 8.08 – 8.03 (m, 4H), 8.0 (s, 2H), 7.94 – 7.89 (m, 8H), 7.7 (d, J = 8 Hz, 4H), 7.6 (d, J = 7 Hz, 2H), 7.5 (br s, 1H), 7.4 (br s 1H), 5.7 (d, J = 8 Hz, 4H), 4.2 (m., 4H), 4,0 (m., 4H), 2,3 (m., 4H). HR-MS (ESI-TOF) m/z Calcd. for $[C_{302}H_{342}F_{72}Fe_2N_{42}O_4Zn_3]^{4+}$: 1522.6912; Found: 1522.6972.

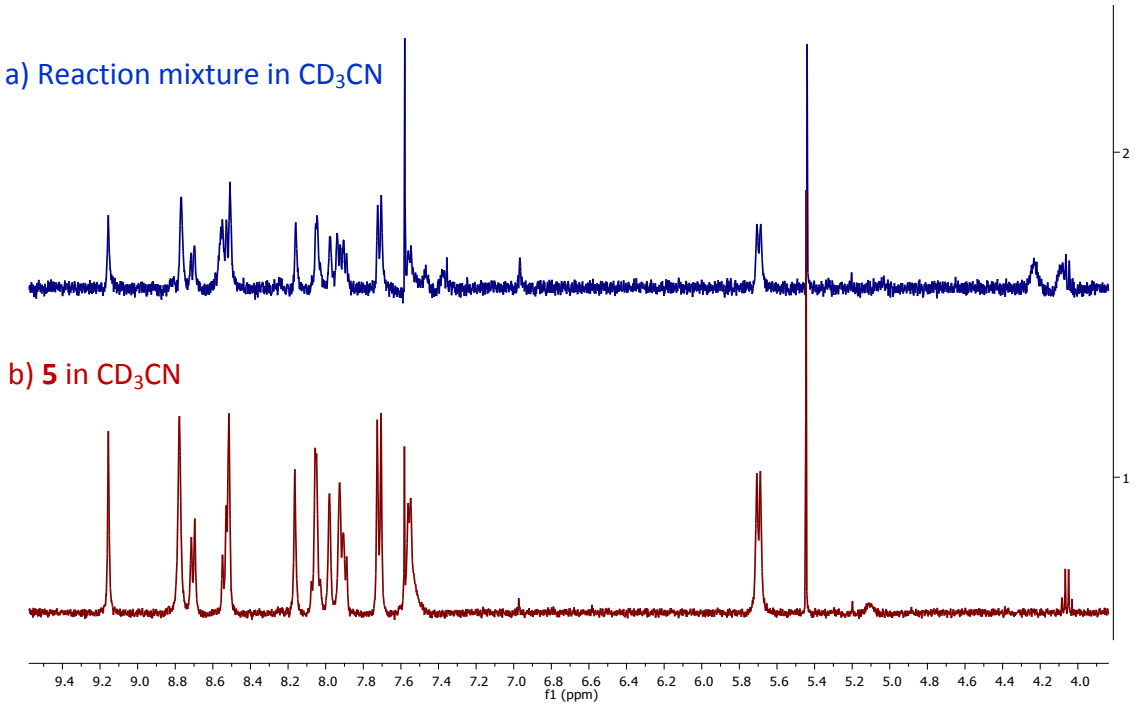

Figure S21. Comparison of the ^{1}H-NMR spectra for the reaction mixture containing [**6** ⊂ **5**] (a-top) and empty **5** (b-bottom).

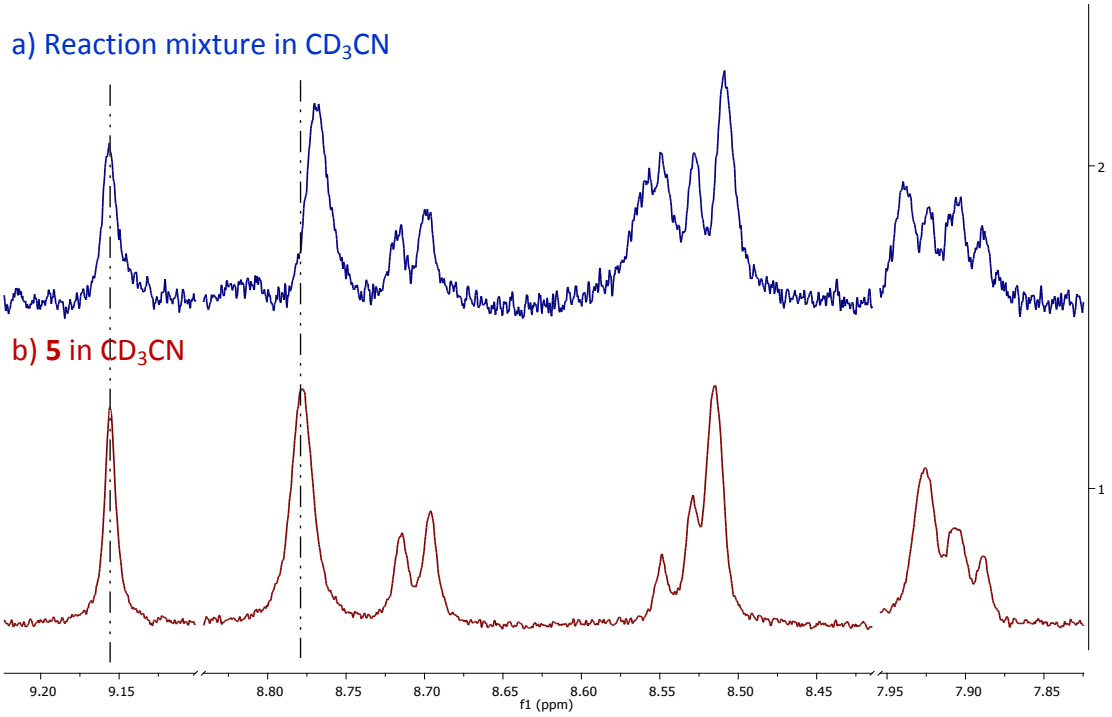

Figure S22. Magnification of aromatic region in the ^{1}H-NMR spectra for the reaction mixture containing [**6** ⊂ **5**] (a-top) and empty **5** (b-bottom), showing the unchanged chemical shift for the imine peak and the differences between Pc-centred nuclei.

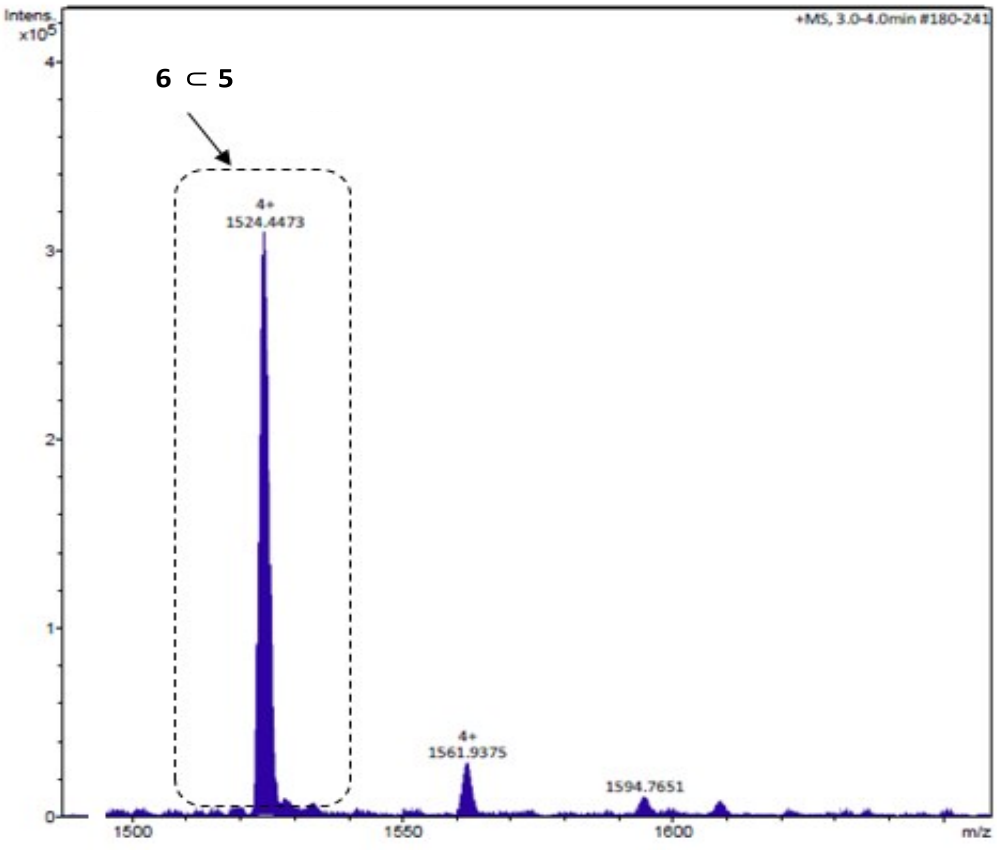

Figure S23. High resolution ESI mass spectrum of **[6 ⊂ 5]**, *m/z* = 1524.4473.

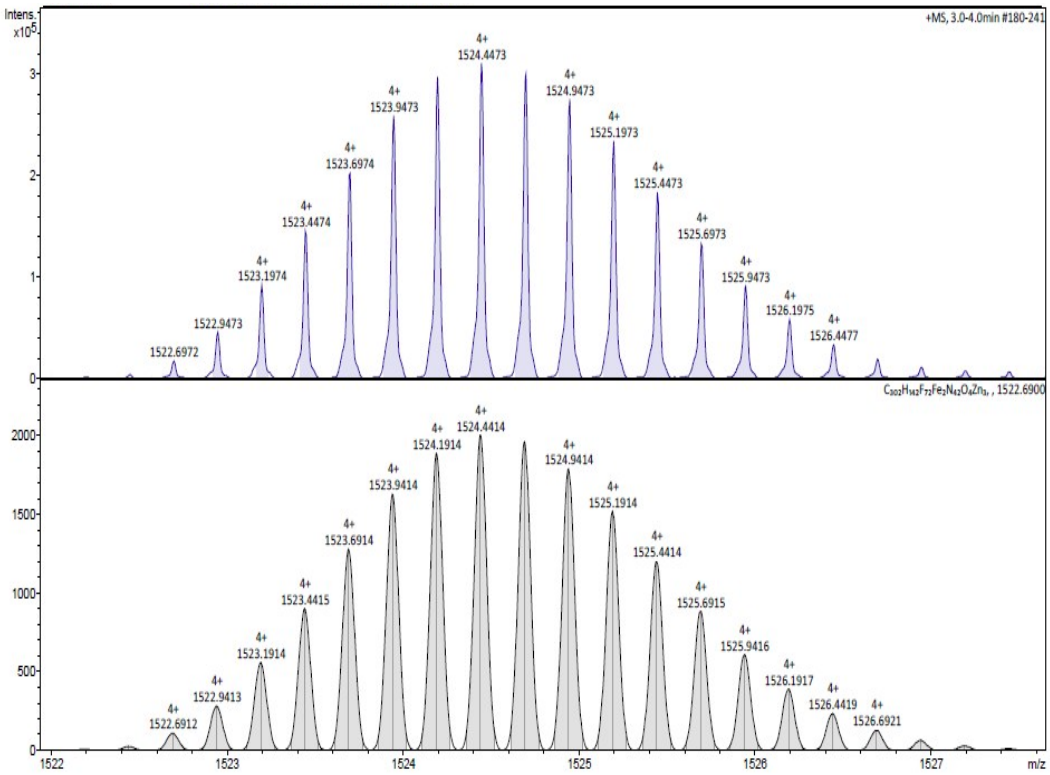

Figure S24. High resolution ESI mass spectrum of **[6 ⊂ 5]**, showing the observed *z* = +4 charge for the peak at *m/z* =1524.4473 (top) compared to the theoretical isotope pattern (bottom).

Titration experiments. The procedure used for UV-vis and fluorescence titrations was the same reported in literature for similar host-guest complexation processes: a 2 mL solution of helicate host **5** (10 µM) in CH_3CN was titrated with a concentrated solution of guest. The total change in concentration of the host was 5.3 – 9.6 % over the course of the titration, and the error involved was assumed to be negligible. Upon each addition, the solution was manually stirred for 1 min before acquiring the spectrum, which allowed equilibrium to be reached between the host and guest. Moreover, the host:guest equivalent ratio goes from 1:0 to 1:4 throughout the titration.

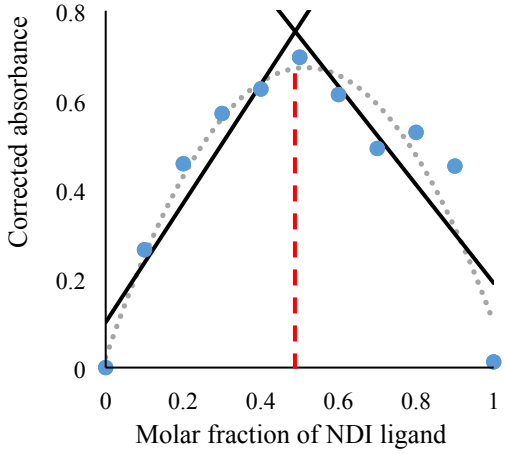

Figure S25. Job's plot diagram of the complex [6 ⊂ 5] (monitored at 692 nm), centered at 0.5 (1:1 stoichiometry), obtained from absorption titration.

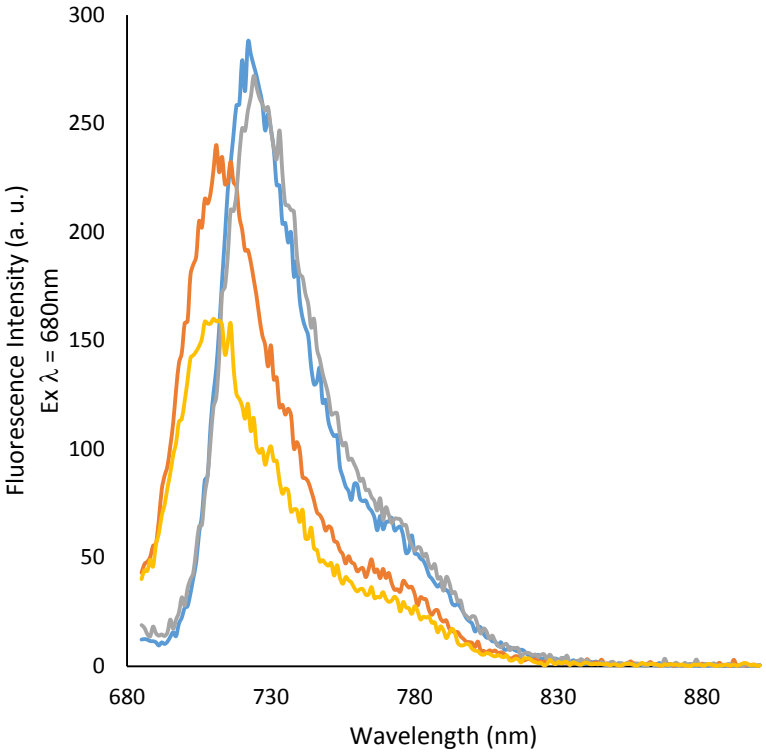

Figure S26. Fluorescence spectra of: Pc **4s** (blue line, 30 μM) in $CHCl_3/CH_3CN$ (1:20); **4s** + **6** (1:1) (grey line, 30 μM) in $CHCl_3/CH_3CN$ (1:20); helicate **5** (dark orange line, 10 μM) in CH_3CN; **5** + **6** (1:1) (light orange line, 10 μM) in CH_3CN.

3. References

(1) E. Fazio, J. Jaramillo-García, G. de la Torre, T. Torres, *Org. Lett.* 2014, **16**, 4706.
(2) F. Billeci, F. D'Anna, S. Marullo, R. Noto, *RSC Adv.* 2016, **6**, 59502.
(3) A. Einstein, *Ann. Phys.* 1906, **324**, 289.
(4) J. T. Edward, *J. Chem. Educ.* 1970, **47**, 261.
(5) M. Wang, K. Wang, C. Wang, M. Huang, X.-Q. Hao, M.-Z. Shen, G.-Q. Shi, Z. Zhang, B. Song, A. Cisneros, *J. Am. Chem. Soc.* 2016, **138**, 9258.
(6) M. J. Burke, G. S. Nichol, P. J. Lusby, *J. Am. Chem. Soc.* 2016, **138**, 9308.
(7) F. Perrin, *J. Phys. Radium* 1936, **7**, 1.
(8) P. H. Elworthy, *J. Chem. Soc.* 1962, 3718.
(9) L. Allouche, A. Marquis, J.-M. Lehn, *Chem. – A Eur. J.* 2006, **12**, 7520.
(10) L. Avram, Y. Cohen, *Chem. Soc. Rev.* 2015, **44**, 586.
(11) K. Mahata, P. D. Frischmann, F. Würthner, *J. Am. Chem. Soc.* 2013, **135**, 15656.
(12) Y. Cohen, L. Avram, L. Frish, *Angew. Chemie Int. Ed.* 2005, **44**, 520.
(13) C. Montoro-García, J. Camacho-García, A. M. López-Pérez, N. Bilbao, S. Romero-Pérez, M. J. Mayoral, D. González-Rodríguez, *Angew. Chemie Int. Ed.* 2015, **54**, 6780.
(14) P. Timmerman, J.-L. Weidmann, K. A. Jolliffe, L. J. Prins, D. N. Reinhoudt, S. Shinkai, L. Frish, Y. Cohen, *J. Chem. Soc., Perkin Trans. 2* 2000, 2077.
(15) G. J. Kleywegt, T. A. Jones, *Acta Crystallogr. Sect. D* 1994, **50**, 178.